Semiconductor plasmonics and metamaterials for IR applications

Patrícia Loren, Pierre Fehlen, Julien Guise, Franziska Barho, Melissa Najem, Fernando Gonzalez-Posada, Stéphane Blin, Laurent Cerutti, Rafik Smaali, Emmanuel Centeno, et al.

Semiconductor plasmonics and metamaterials for IR applications

P. Loren[a], P. Fehlen[a,b], J. Guise[a], F. Barho[a], M. Najem[a], F. Gonzalez-Posada-Flores[a], S. Blin[a], L. Cerutti[a], R. Smaali[c], E. Centeno[c] and T. Taliercio*[a]
[a]IES, Univ Montpellier, UMR CNRS 5214, Montpellier, France; [b]NSE3 (CNRS UMR3208) Institut franco-allemand Saint-Louis; [c]Universite Clermont Auvergne, CNRS, SIGMA Clermont, Institut Pascal, F-63000 Clermont-Ferrand, France

ABSTRACT

In this paper, III-IV semiconductors are demonstrated as strong candidates for plasmonics applications in the Mid-IR. The perfect absorbers (PA) fabricated with heavily doped semiconductors features strong coupling between Fabry-Perot and localized surface plasmon modes. Also, anisotropic nano-antenna fabricated at the top surface yield a huge anisotropy to the polarized light. The fabricated PA with 2D periodic arrays of rectangular nano-antenna is presented, where the rectangular shape allows one to excite localized surface plasmon resonances (LSPR) at different wavenumbers depending on the polarization of the incident light. Preliminary results of the bio-functionalization through phosphonic acid are shown for the PA aditionnally. Furthermore, it becomes clear that it is possible to detect bio-molecules of interest even far in the infrared on a very small surface and with a few hundreds of nano-antenna.

Keywords: Heavily doped semiconductor, Biosensing, active plasmonics, mid-infrared spectroscopy, THz spectroscopy

1. INTRODUCTION

Plasmonics is one of the main fields of nanophotonics exploiting the coupling between photons and the collective oscillations of free carriers at metallic surfaces or nanostructures. The surface plasmon polariton is the resulting quasi-particle with strong electric field confinement and huge electric field enhancement at the metal surface. These main features offer potential applications from biosensing to solar cell technologies. Heavily doped semiconductors, such as III-V[1], Ge[2], Si[3], or oxides[4], are designed metals that allow the control of their plasmonic properties from the THz up to the near-infrared spectral range. These materials are particularly well suited for bio-sensing applications because their plasmonic resonance covers the fingerprint spectral range of biomolecules (500-1600 cm^{-1})[5]. Several geometries of plasmonic structures have been tested to obtain the maximum biosensing sensitivity[6]. One of the best suited is the perfect absorber (PA). PA consists of a back reflector deposited on a substrate to suppress all transmitted light and a multi-layered structure deposited on the back reflector to allow impedance matching with the air to suppress all reflected light[7] (Fig. 1-a). Thus, because the PA does not reflect nor transmit light, it absorbs all incident light, and thanks to 2nd Kirchhoff's law[8] which states the equality of absorptance and emittance, the ratio of absorbed, respectively emitted, to the incident radiant power, the PA also acts as a perfect emitter. In terms of biosensing applications, PA can either enhance the absorption of rovibrational modes of molecules with surface-enhanced infrared absorption (SEIRA) spectroscopy[9] or enhance the thermal emission of molecules with surface-enhanced thermal emission spectroscopy[10]. In this work, we will be focusing on the fabrication of PA based on heavily doped semiconductors for long-wavelength infrared biosensing using the SEIRA technique.

2. SAMPLE FABRICATION AND EXPERIMENTAL SETUP

2.1 Sample fabrication

The sample, based on antimonide alloys, is grown by solid source molecular beam epitaxy on n-type GaSb substrate. First, a buffer layer of 210 nm of nonintentionally doped GaSb is grown. Then the perfect absorber is grown with a back mirror of Si-doped $InAs_{0.91}Sb_{0.09}$, a spacer of GaSb, and a top layer of Si-doped $InAs_{0.91}Sb_{0.09}$ (Fig. 1-a). The InAsSb:Si alloy is lattice-matched to the GaSb substrate allowing to reduce the point defect density and to improve the optical properties of this alloy. The doping level of the InAsSb:Si is 6 10^{19} cm^{-3} and the thicknesses of the back mirror, the spacer and the top layer are respectively m = 988 nm, s = 350 nm, and e = 100 nm. The spacer and the nanostructured top

layer are the structures that allow the impedance matching to the air to cancel the reflected beam. The doping level of InAsSb:Si is measured by the Brewster mode technique[11].

The nano-antenna fabrication process flow is as follow: After careful cleaning of the sample by acetone in an ultrasonic bath for 2 min., then by isopropanol (IPA) alcohol for 2 min. and by abundantly rinsing with IP and dried by N_2 flux, the sample is annealed for 10 min. at 110°C. The photoresist PMMA is spread at 6000 rpm and annealed for 1 min and 30 s at 180°C. E-beam lithography is performed by a modified JEOL microscope equipped with a RAITH system. It allows to pattern 2-D periodic arrays of rectangle nano-antenna into the photoresist with pitches Λ_x = 810 nm and Λ_y = 1000 nm, and nano-antenna size of w = 450 nm and l = 700 nm. The writing parameters are 14.67 µC/cm^2, <20 pA, 20 nm, and > 1 µs respectively for the dose, the beam current, the step-size, and the dwell time. The sample is then dipped into the developer MIBK (3:1) for 30 s, rinsed with IPA for 30s, before being dried with a N_2 flux. Then, an aluminium film is deposited on the surface followed by a lift-off, the remaining film is the mask that protects the surface sample. The dry etching of the antennas is performed by the induced-coupled-plasma-reactive-ion-etching (ICP-RIE) Oxford system for 2 min with the following recipes: 60°C, 5 Torr, 25 sccm, 7.5 10^{-9} Torr, 50W, 500W respectively for the temperature, pressure, Ar flow, the pressure, the RF power, and the ICP power. To avoid etching of the GaSb substrate, the dry etching is stopped a few nm over the interface between InAsSb and GaSb, and finished with a wet etching using citric acid/H_2O_2 at (2:1) for 12 s, rinsed with DI, and dried with N_2. The sample is cleaned by acetone in an ultrasonic bath for 2 min., then by isopropanol (IP) alcohol for 2 min. and by abundantly rinsing with IP and dried by N_2 flux. Finally, an oxygen plasma for 3 min is performed to remove the residual photoresist.

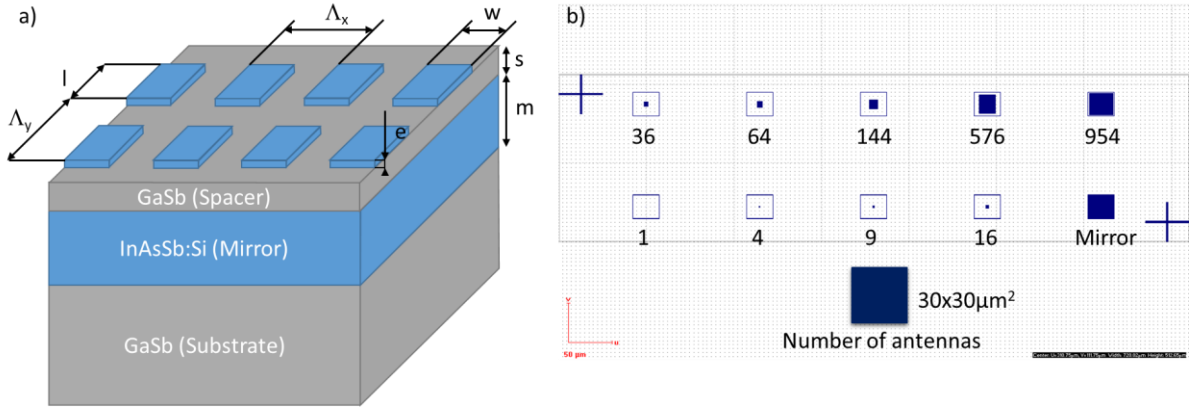

Figure 1. a) Schematic of the perfect absorber. It is a multilayer of GaSb and heavily doped InAsSb:Si. The thickness are m = 988 nm for the InAsSb:Si back mirror, s = 385 nm for the spacer of GaSb, and e = 100 nm for the top layer of InAsSb:Si. The pitches of the 2-D periodic arrays are Λ_x = 810 nm and Λ_y = 1000 nm. The sizes of the nano-antenna are w = 450 nm and l = 700 nm. These values can slightly (+/- 10%) vary from one zone to the other. b) Schematic of the surface sample. The squares are 30 x 30 µm^2. They contain from 1 to 954 nano-antenna. The number of nano-antenna is indicated below the squares. The mirror corresponds to an unpatterned PA layer structure. It will be used as the reference for differential reflectance measurements.

Fig. 1-b schematizes the periodic arrays of rectangular nano-antenna etched on the top surface layer of InAsSb:Si. The nano-patterned areas are delimited by the 30 x 30 µm² small blue squares in the schema. The number of nano-antenna in the squares is labelled below it. The number of nano-antenna varies from 1 to 954. The label mirror consists of an un-etched top surface layer of InAsSb:Si. It will be used as a background signal for a reduce spectral range (< 1850 cm^{-1}) of the reflectance spectra.

2.2 Experimental setup

The fabricated samples were characterized using a Brucker Vertex 70 Fourier transform infrared (FTIR) spectrometer equipped with a globar mid-IR source, a KBr beam splitter, and MCT detector D315-025. Two experimental techniques have been used. The Brewster mode experimental technique[11] allows to extract the doping level of the InAsSb:Si, and a Hyperion 3000 microscope coupled to the FTIR is used to obtain the reflectance spectra of the 2-D periodic arrays. Cassegrain objectives have been used with a magnification of x15 or x36. The results presented in the following main results are obtained with the x15 objective. To limit the spatial zone at the surface of the sample, for example, a 30 x 30 µm^2 area, we used the confocal setup of the Hyperion 3000 microscope with an internal knife-edge aperture. The spatial

limitation reduces the signal-to-noise ratio (SNR). To improve the SNR, 1000 accumulations of direct interferograms of the background signal and the signal from the sample were performed.

Reflectance spectra are obtained using a gold mirror as a background signal for the mid-IR spectral range. It is also possible to use the zone labeled as "mirror" in Fig. 1-b to perform the reflectance measurements but for a spectral range limited to wavenumbers below 1750 cm^{-1}. This avoids large displacements in the sample and additional focus on the gold mirror and improves therefore the SNR.

3. SAMPLE CHARACTERIZATION AND NANO-ANTENNA OPTICAL PROPERTIES

3.1 Sample characterization

Fig. 2 shows a schematic of the surface sample to localize the spatial zone where the scanning electron microscope (SEM) images are taken. The zones are labeled A1 and A2 for the zones with 1 and 4 nano-antenna. The zone labeled B1 to B5 correspond to the zones with respectively 36, 64, 144, 576, and 954 nano-antenna. The associated SEM images of the zones B5 (red rectangle), A1 (green rectangle), and A4 (blue rectangle) zones are represented in Fig. 2. The shape of the nano-antenna is close to the expected rectangle. The pitches along the x- and y-axis are 810 nm and 1000 nm. The sizes of the rectangle are w ~ 450 nm and l ~ 700 nm. The second layer seen on the top of the rectangles are defects caused by the e-beam writing.

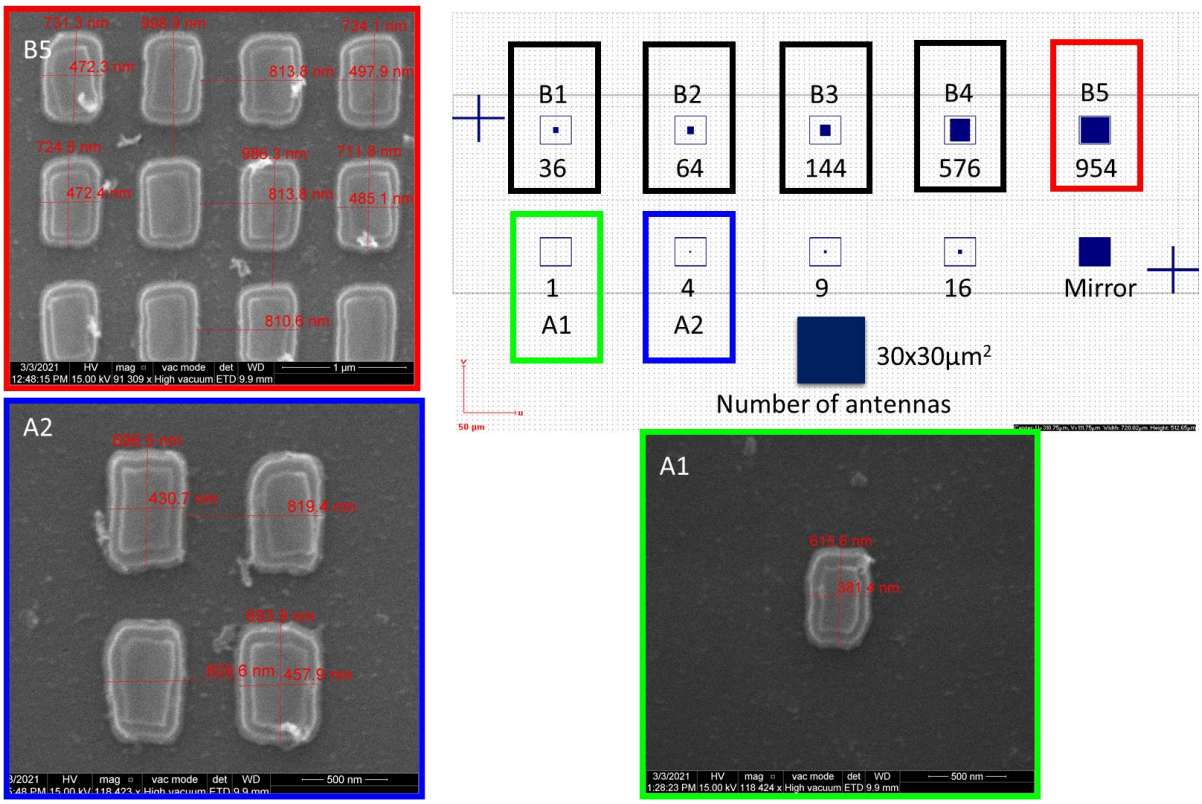

Figure 2. Schematic of the nanostructured top layer of the perfect absorber structure. Compared to Fig. 1-b, we have added labels A1, A2, and B1, …, B5 to spot the spatial zone studied by SEM or by FTIR spectroscopy. A1, A2, and B5 are the SEM images of the top layer of the sample.

3.2 Optical properties

The different spatial zones, B2, B3, B4, and B5 have been studied by FTIR spectroscopy (Fig. 3-c). The reflectance spectra of the B5 zone obtained with a gold mirror as the background signal are shown in Fig. 3-a. The low SNR of the spectra is due to the small surface studied, 30x30 μm^2. The reflectance spectrum under x-polarized light (see inset of Fig. 3a for the polarization directions) is the black curve. It corresponds to the excitation of the localized surface plasmon resonance, LSPR-x, of the short axis of the rectangle nano-antenna. The reflectance spectrum under y-polarized light is

the red curve. It corresponds to the excitation of the localized surface plasmon resonance of the long axis of the rectangle nano-antenna. In both spectra, two main spectral zones are distinguished. The first one is for wavenumbers larger than 2000 cm^{-1}. It corresponds to the dielectric behavior of the InAsSb:Si. There are some interference patterns due to the stacked layers system (InAsSb:Si/GaSb). For wavenumbers smaller than 2000 cm^{-1}, InAsSb:Si behaves like a metal. In this second spectral range, the structure behaves as a perfect absorber, if the nanostructures of the top layer have adapted sizes. This is not the case here since the nano-antenna are too large. However, we identify the spectral signature at 580 cm^{-1} under x-polarized light. For the y-polarized light, the wavenumber of the resonance is far in the infrared, out-of-range of the MCT detector of the FTIR coupled to the microscope. The cavity mode associated with the metal-insulator-metal structure, which is the building block of the perfect absorber, is at 1060 cm^{-1}. The large wavenumber mismatch between LSPR and the cavity mode shows us that we are far from the strong coupling regime[9]. In these conditions, the perfect absorption is not reached because the electric field of the cavity mode is not maximum at the surface when the LSPR absorbs light.

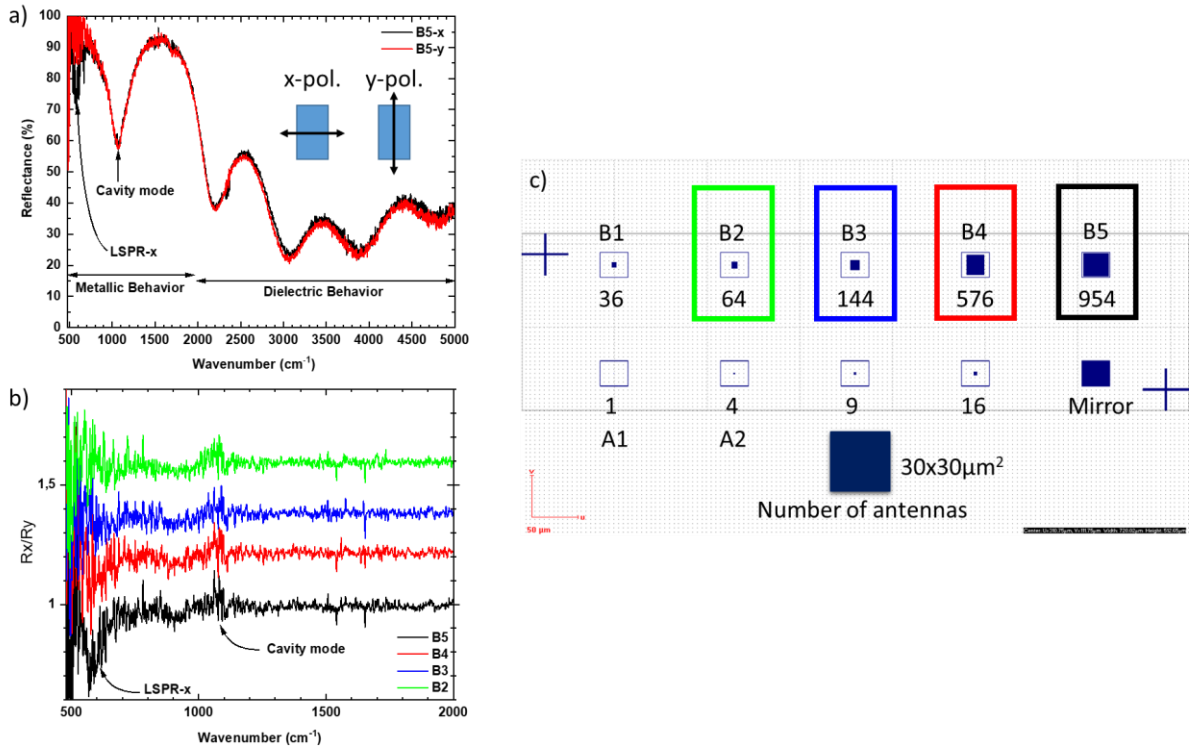

Figure 3. a) Reflectance spectra of the B5 zone with a polarization of the light (the electric field direction) along the x-axis (black curve) or along the y-axis (red curve). The background signal is obtained with a gold mirror. b) Ratio between the reflectance spectra obtained under x- or y-polarized light for the spatial zones B2, B3, B4, and B5. The background signal is obtained on the mirror of the sample. c) Schematic of the nanostructured top layer of the perfect absorber structure.

Fig. 3-b shows the spectra of the ratio between reflectance spectra under x-polarized and y-polarized light for the spatial zones B2 (green curve), B3 (blue cure), B4 (red curve), and B5 (black curve). The background signal is obtained with the "mirror". We can observe the spectral signature of the LSPR-x between 520 cm^{-1} and 700 cm^{-1} for zones B4 and B5. It is possible to detect less than 576 nano-antenna with the current experimental setup. Of course, it is possible to decrease this number working in the most adapted spectral range for this detector near 1000 cm^{-1}. We did not observe a significant signal in the other zones. Further investigations are needed to detect signal from less nano-antenna.

3.3 Bio-functionalization with Phosphonic Acid

We investigate the biosensing properties of the PA introducing bio-functionalization with 11-Hydroxyundecylphosphonic acid (HUPA)[12]. The chemisorption experiment started with dissolving the phosphonic acid-based coupling agent in 10 ml of ethanol to obtain 1 mM solutions. To rinse the surfaces from contaminations, the cleaved III–V samples were sonicated for 5 min. in acetone and IPA. The process then consists in exposing the III–V

surfaces for 5 min to O_2-plasma at 300 W and 50 mbar (PicoPCCE, Diener electronics) and then immersing the samples in the solution for 24 h. After the immersion, all samples were baked for 12 h in an oven at 120°C (UF260, Memmert) to increase the grafting stability. Finally, all samples were rinsed with ethanol and sonicated for 5 min. in acetone and IPA.

Fig. 4-a shows the reflectance spectra of the zone B4 obtained under x-polarized light. The background signal is obtained with the "mirror". The black curve corresponds to the reflectance spectrum of B4 without functionalization. The LSPR-x is centered at 590 cm^{-1}. The red curve corresponds to the reflectance spectrum of B4 with functionalization. The position of LSPR-x is located at the same wavenumber, 590 cm^{-1}. No redshift is measurable. However, we can see a zigzag appearing at the low energy of the LSPR-x which is exactly at the wavenumber of the vibrational mode of the phosphonic acid, 543 cm^{-1}, circled in green. The shape modification of the absorption line, due to phase modification between the LSPR-x and the vibrational mode of the phosphonic acid, is the typical behavior of the Fano-like mechanism involved in SEIRA[13].

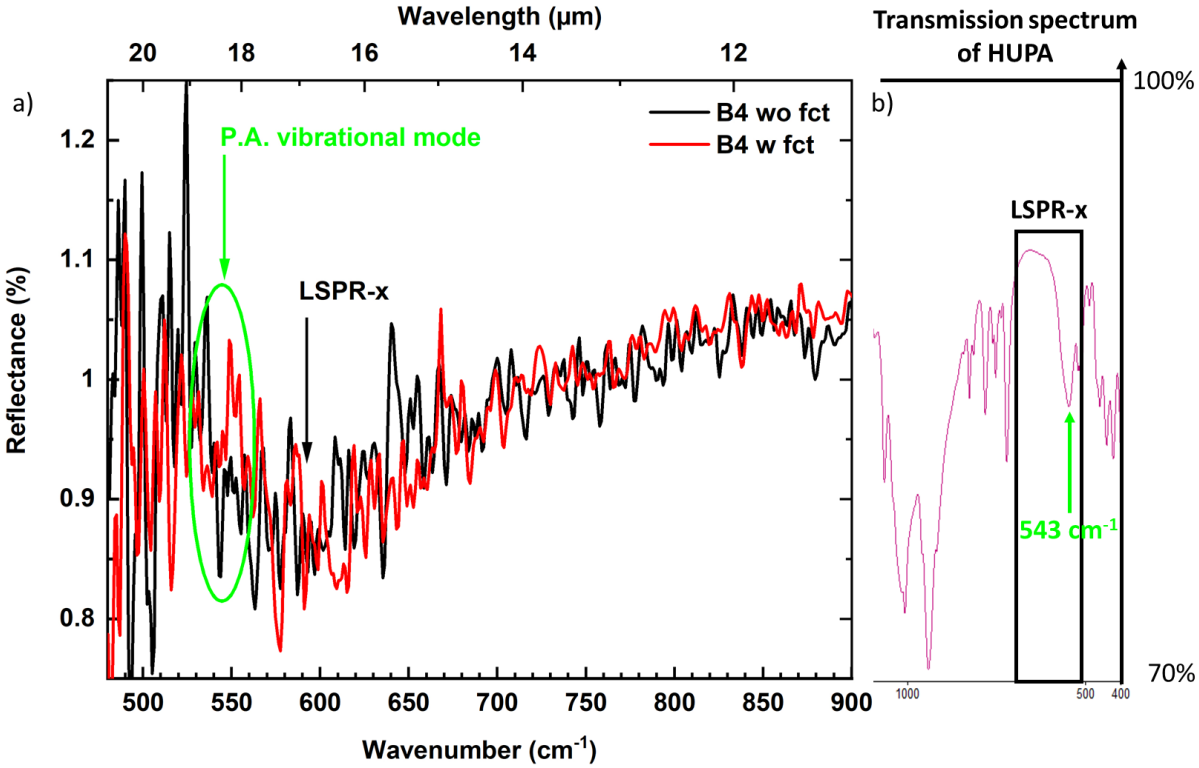

Figure 4. a) Reflectance spectra of zone B4 with a polarization of the light along the x-axis. The background signal is obtained with the "mirror". The black curve corresponds to the reflectance spectrum of B4 without functionalization whereas the red curve corresponds to the reflectance spectrum of B4 with functionalization. The LSPR-x is pinned at 590 cm^{-1} and the position of one vibrational mode of the phosphonic acid is circled in green at 543 cm^{-1}. b) Transmission spectrum of the 11-Hydroxyundecylphosphonic acid (HUPA). The spectral range covered by the LSPR-x of B4 is delimited by the black rectangle. The main vibrational mode of the phosphonic acid in this spectral range is at 543 cm^{-1}.

Fig. 4-b shows the transmission spectrum of the phosphonic acid with the targeted vibrational mode at 543 cm^{-1} (vertical green arrow). The spectral range covered by the LSPR-x is delimited by the black rectangle. The identification of this vibrational mode in the reflectance spectrum of Fig. 4-a is unobvious because the SNR is too weak and close to the noise amplitude. Additional investigation should be performed to confirm these preliminary measurements.

4. CONCLUSION

The capability of III-V semiconductors for plasmonics application in the far-infrared spectral range was demonstrated. The perfect absorbers fabricated with doped semiconductors demonstrate efficient coupling of localized plasmon modes to the incident light thanks to the strong coupling effect between the Fabry-Perot resonance and the LSPR. We have designed rectangular nano-antenna that allow to reach a wavenumber of 580 cm^{-1} for the LSPR-x associated to the short

axis of the nano-antenna whereas the LSPR-y excited along the long axis is probably far in the infrared. We have functionalized the surface of the PA with phosphonic acid with a strong vibrational mode at 543 cm^{-1} corresponding to the low wavenumber part of the LSPR-x. A weak Fano-like resonance appears at 543 cm^{-1} in the broad LSPR-x of the nano-antenna. This spatial zone contains just 576 nano-antenna. Additional experimental investigation is necessary to confirm the SEIRA signal obtained with these nano-antenna. Moreover, it would be of interest to further reduce the number of nano-antenna within a spatial zone for SEIRA measurements.

FUNDING SOURCES

This work was partially funded by the French Investment for the Future Program (EquipEx EXTRA, ANR 11-EQPX-0016), the French ANR (SUPREME-B ANR 11-14-CE26-0015), the Occitanie Region (ESR_PREMAT – 00238 / Prématuration 2019 SEA), and the "Investissements d'avenir" programme with the reference ANR-16-IDEX-0006 (EnviroDisorders_AAPMUSE2020). F. Pichot, J.-M. Peiris, and F. Mirabel are acknowledged for technical support at the cleanroom facilities of Université de Montpellier.

REFERENCES

[1] N'Tsame Guilengui, V., Cerutti, L., Rodriguez, J.B., Tournié, E., Taliercio, T., "Localized surface plasmon resonances in highly doped semiconductors nanostructures," Appl. Phys. Lett. 101, 161113 (2012).

[2] Biagioni P, Frigerio J, Samarelli A, Kevin Gallacher, K., Baldassarre, L., Sakat, E., Calandrini, E., Millar, R. W., Giliberti, V., Isella, G., Paul, D. J., Ortolani, M., "Group-IV midinfrared plasmonics," J. Nanophot. 9, 093789 (2015).

[3] Mu, J., Soref, R., Kimerling, L. C., Michel, J. "Silicon-on-nitride structures for mid-infrared gap-plasmon waveguiding," Appl. Phys. Lett. 104, 031115 (2014).

[4] Hierro, A., Montes Bajo, M., Ferraro, M., Tamayo-Arriola, J., Le Biavan, N., Hugues, M., Ulloa, J. M., Giudici, M., Chauveau, J.-M., and Genevet, P, "Optical Phase Transition in Semiconductor Quantum Metamaterials," Phys. Rev. Lett. 123, 117401 (2019).

[5] Taliercio, T., and Biagioni, P., "Semiconductor infrared plasmonics," Nanophotonics 8, 949–990 (2019).

[6] Neubrech, F., Huck, C., Weber, K., Pucci, A., Giessen, H., "Surface enhanced infrared spectroscopy using resonant nanoantennas," Chem. Rev. 117, 5110–5145 (2017).

[7] Greffet, J.-J., Carminati, R., Joulain, K., Mulet, J.-P., Mainguy, S., Chen, Y., "Coherent Emission of Light by Thermal Sources," Nature 416, 61 (2002).

[8] Chan, D. L. C., Soljacic, M., Joannopoulos, J. D., "Thermaĺ Emission and Design in One-Dimensional Periodic Metallic Photonic Crystal Slabs," Phys. Rev. E - Stat. Nonlinear, Soft Matter Phys. 74, 1−9 (2006).

[9] Barho, F. B., Gonzalez-Posada Florès, F., Cerutti, L. and Taliercio, T., "Highly doped semiconductor metamaterials for mid-infrared multispectral perfect absorption and thermal emission," Adv. Optical Mater. 1901502 (2020).

[10] Barho, F. B., Gonzalez-Posada Florès, F., Mezy, A., Cerutti, L. and Taliercio, T., "Surface-Enhanced Thermal Emission Spectroscopy with Perfect Absorber Metasurfaces," ACS Photonics 6, 1506−1514 (2019).

[11] Taliercio, T., N'Tsame Guilengui, V., Cerutti, L., Tournié, E., Greffet, J. J., "Brewster "mode" in highly doped semiconductor layers an all-optical technique to monitor doping concentration," Opt. Express 22, 24294 (2014).

[12] Bomers, M., Mezy, A., Cerutti, L., Barho, F., Gonzalez-Posada Flores, F., Tournié, E., Taliercio, T., "Phosphonate monolayers on InAsSb and GaSb surfaces for mid-IR plasmonics," Applied Surface Science 451, 241–249 (2018).

[13] Milla, M. J., Braho, F., Gonzalez-Posada, F., Cerutti, L., Charlot, B., Bomers, M., Neubrech, F., Tournié, E., Taliercio, T., "Surface-enhanced infrared absorption with Sidoped InAsSb/GaSb nano-antennas," Optics Express 25, 26651 (2017).